Concomitant Double Ion and Electron Populations in the Earth's Magnetopause Boundary Layers From Double Reconnection With Lobe and Closed Field Lines

Benoit Lavraud, Christian Jacquey, Timothée. Achilli, Stephen A. Fuselier, Elena Grigorenko, Tai D. Phan, Marit Øieroset, James Mcfadden, Vassilis Angelopoulos

HAL Id: insu-03678196
https://insu.hal.science/insu-03678196

Submitted on 25 May 2022

Concomitant Double Ion and Electron Populations in the Earth's Magnetopause Boundary Layers From Double Reconnection With Lobe and Closed Field Lines

Benoit Lavraud[1] [iD], **Christian Jacquey[1]** [iD], **Timothée Achilli[1]**, **Stephen A. Fuselier[2,3]** [iD], **Elena Grigorenko[4]** [iD], **Tai D. Phan[5]** [iD], **Marit Øieroset[5]** [iD], **James McFadden[5]**, and **Vassilis Angelopoulos[6]** [iD]

[1]Institut de Recherche en Astrophysique et Planétologie, Université de Toulouse, CNRS, UPS, CNES, Toulouse, France, [2]Southwest Research Institute, San Antonio, TX, USA, [3]University of Texas at San Antonio, San Antonio, TX, USA, [4]Space Research Institute of the Russian Academy of Sciences, Moscow, Russia, [5]Space Sciences Laboratory, University of California, Berkeley, CA, USA, [6]Institute of Geophysics and Planetary Physics, University of California, Los Angeles, CA, USA

Abstract While double ion populations, with a cold population originating from the solar wind and a hotter one from the magnetosphere, are frequently observed in the low-latitude boundary layers at the Earth's magnetopause, similar double electron populations are observed less often. A preliminary study of magnetopause crossings characteristics was used to determine the typical locations and energy spectra of ion and electron populations near the magnetopause. Then, we set up an automated detection algorithm for identifying regions with concomitant double populations in both ion and electron energy spectra. The statistical study was carried out on 7 years of Time History of Events and Macroscale Interactions during Substorms particle data, to determine the interplanetary magnetic field conditions in the upstream solar wind for these double populations. The results suggest that such concomitant ion and electron double population boundary layers form preferentially in the subsolar region and under northward interplanetary magnetic field but with a significant B_Y component. We interpret this finding as the result of reconnection of the same magnetosheath field line in both hemispheres with at least one end reconnecting in its hemisphere at lower latitude with a closed magnetospheric field line that already contains a hot electron source.

1. Introduction

The magnetopause, the outer boundary of the magnetosphere, is a thin current sheet separating the solar wind plasma from the geomagnetic field. Coupling between the solar wind and the magnetosphere is largely driven by magnetic reconnection occurring at different locations on the magnetopause, as a function of the solar wind properties and in particular the interplanetary magnetic field (IMF) orientation. For southward IMF, antiparallel to the geomagnetic field on the front of the magnetosphere, reconnection occurs near the subsolar magnetopause (Dungey, 1961). When the IMF is directed northward, by contrast, antiparallel solar wind and magnetospheric lobe field lines reconnect at higher latitudes poleward of the cusps (Gosling et al., 1991; Kessel et al., 1996; Lavraud et al., 2002). The reconnected field lines in this case convect sunward, then dawnward or duskward and eventually tailward, away from the reconnection site along the flanks (e.g., Lavraud et al., 2005; Ogino et al., 1994).

Under southward IMF, boundary layers observed at low latitudes on the dayside are explained by magnetic reconnection in the nearby subsolar region. The boundary layers are characterized by a mixing of plasmas from the magnetosheath and magnetosphere (with intermediate temperature) and enhanced flows (often referred to as *jets* and consistent with the Walén test [e.g., Paschmann et al., 1979]). Because, by contrast, magnetic reconnection in the subsolar region is not expected under northward IMF (owing to parallel magnetic fields there), the frequent observation of boundary layers under such conditions near the subsolar magnetopause has long remained problematic. Several processes have been suggested to explain their formation, with varying success: (1) particle diffusion through wave-particle interactions, which may not explain boundary layers thicker than 0.5 R_E (Treumann et al., 1995; Wing et al., 2014), (2) the Kelvin-Helmholtz (KH) instability, which cannot explain their formation in the subsolar region owing to the lack of velocity shear there (i.e., basic ingredient for the KH instability; Fairfield et al., 2000; Foullon et al., 2008;

Hasegawa et al., 2004; Nykyri et al., 2006; Taylor & Lavraud, 2008), and (3) double high-latitude reconnection (Fuselier, Frahm, et al., 2014; Lavraud et al., 2006; Onsager et al., 2001; Song & Russell, 1992). This latter possibility for dayside boundary layer formation under northward IMF implies a double reconnection process of the same magnetosheath field lines, poleward of the cusps, in both the southern and northern lobes. This process can create newly closed field lines with trapped, dense plasma of solar wind origin, as also suggested by global simulations (Li et al., 2008; Ogino et al., 1994; Raeder et al., 1997).

Reconnection at the magnetopause also produces a unique electron signature: heated electrons streaming on open field lines that lie sunward of the magnetopause current layer. This electron signature is used widely to investigate the topology of magnetic field lines at planetary magnetopauses (Badman et al., 2013; Fuselier et al., 1995, 1997, 2012; Fuselier, Petrinec, et al., 2014; Lavraud, Thomsen, et al., 2005; Lavraud et al., 2006; McAndrews et al., 2008; Onsager et al., 2001). For instance, evidence for double high-latitude reconnection under northward IMF includes observations of heated, bidirectional streaming electrons at high latitudes in the boundary layer sunward of, but adjacent to, the magnetopause (called the Magnetosheath Boundary Layer; Lavraud, Thomsen, et al., 2005; Lavraud et al., 2006; Onsager et al., 2001). However, observations at lower latitudes in the Magnetosheath Boundary Layer often show unidirectional streaming electrons. These observations suggest that only one high-latitude reconnection site is active (Fuselier et al., 1995). Fuselier et al. (2012) suggested that the differences in the properties of streaming electrons at high and low latitudes can be explained if reconnection is not simultaneous in the two hemispheres. If time allows, a field line reconnected in one hemisphere may drape around the magnetopause and partially sink into the magnetosphere before reconnecting in the opposite hemisphere. Therefore, although the magnetic field lines eventually reconnect in both hemispheres, this short delay between both reconnections is sufficient for the field line to convect away from the subsolar region and explain the lack of bidirectional electrons there.

As a result of the aforementioned processes, the dayside magnetopause boundary layers typically contain both cold electron and ion populations of (shocked) solar wind origin. The magnetopause boundary layers also typically contain a hot ion population of magnetospheric origin. The presence of a hot electron population of magnetospheric origin is, however, seldom observed. Such cases have been reported mostly for northward IMF, for instance in Øieroset et al. (2008; see also Hasegawa et al., 2003). Øieroset et al. (2008) explained their presence by a low-latitude boundary layer (LLBL) formation scenario wherein the capture of magnetosheath plasma onto closed field lines is made by consecutive tailward-of-the-cusp reconnection in one hemisphere and equatorward-of-the-cusp reconnection in the other hemisphere (see also Cowley, 1981, Onsager et al., 2001, and Chandler et al., 2008, for example). This process has not been documented much in the literature for the case of the Earth's magnetosphere.

In the present paper, we report a statistical study of the occurrence of double electron and ion populations in the LLBL to determine which physical process may explain their relatively rare presence in the dayside LLBL. For that purpose, we search for a double peak in fluxes at energies typical of the magnetosheath and magnetosphere, for both ions and electrons. From now on, we refer to these as ion and electron double population boundary layers (DPBLs).

2. Event Illustration

In this work, the primary data are from the Time History of Events and Macroscale Interactions during Substorms (THEMIS) multispacecraft mission. We use in particular magnetic field measurements from the flux-gate magnetometers (Auster et al., 2008) and particle measurements from the electrostatic analyzers (ESAs; McFadden et al., 2008). In this section, we present an overview of a magnetopause boundary layer crossing which occurred on 3 June 2007. This event is representative of DPBL events analyzed here. It was studied in details by Øieroset et al. (2008), who focused on the more general formation mechanism of the LLBL under northward IMF. Figure 1, similar to Figure 2 Øieroset et al. (2008), displays data from the THEMIS-A spacecraft during the event. It displays in panel (a) the IMF data from the Advanced Composition Explorer spacecraft in the solar wind, time shifted by 3,450 s as determined from the correlation of Advanced Composition Explorer and THEMIS B data (which is in the magnetosheath during most of that interval).

Panel (a) shows that the IMF has a dominant northward orientation until the magnetopause crossing at ~17:11 UT (vertical dashed line), albeit with a significant negative B_Y component (consistent with the
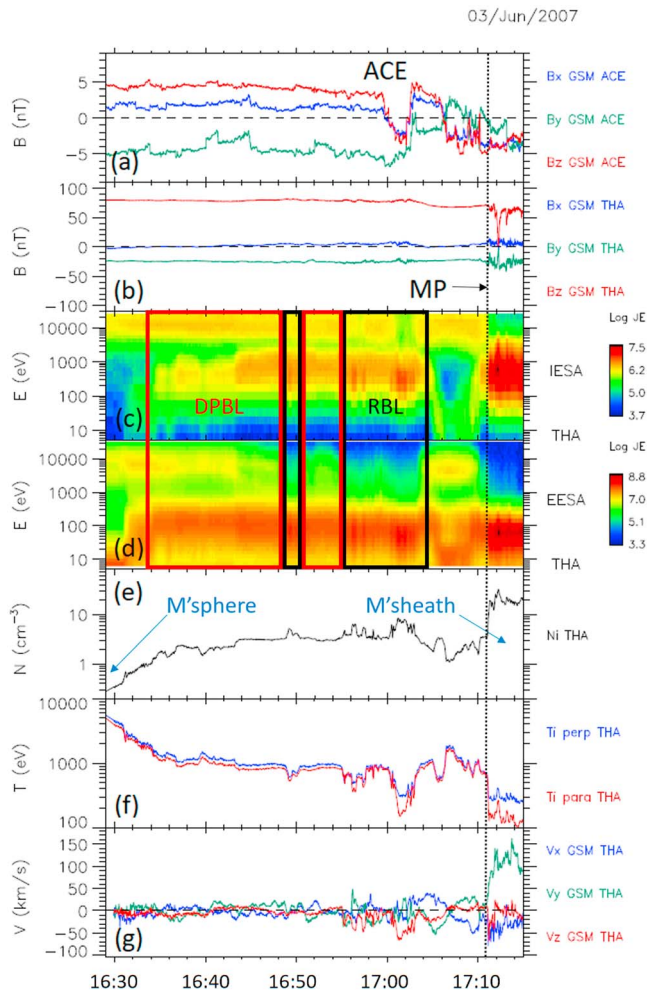
Figure 1. Typical boundary layer crossing under northward interplanetary magnetic field as recorded by Time History of Events and Macroscale Interactions during Substorms A. (a) Time-shifted (3,450 s) interplanetary magnetic field measured by Advanced Composition Explorer. (b–h) TH-A measurements of the (b) magnetic field, (c) ion and (d) electron energy spectrograms (in eV/(cm^2-s-sr-eV)), € ion density, (f) parallel and perpendicular temperature and (g) velocity components in GSM coordinates. The magnetopause, magnetosphere, and magnetosheath are noted. Colored rectangles in panels (c) and (d) mark the electron and ion double population boundary layer, as well as the regular boundary layer with only a double population observed in the ion spectrogram. This figure is similar to Figure 2 in Øieroset et al. (2008).

results of our statistical analyses that are described later). The boundary layer interval of interest (including both the red and black rectangles in panels [c] and [d]) is observed in between the magnetosphere itself (at the beginning of the interval, with low density and only high-energy electrons and ions; M'sphere on panel [e]), and the magnetopause (at ~17:11 UT). Overall, it shows a zone of mixed populations, with both hot magnetospheric and colder magnetosheath ions between the magnetosphere and the magnetosheath, lasting for more than half an hour. In this region, ion densities and temperatures are intermediate between magnetospheric and magnetosheath values (panels [e] and [f]). In addition to these two ion populations, we also identify in panel (d) the presence of mixed electron populations of both magnetospheric and magnetosheath origin; these times are specifically marked with the red rectangle and termed DPBL (note that the rectangles in Figure 1 are only meant to guide the eye). The key unknown here, which is only alluded in past works (e.g., Øieroset et al., 2008; Onsager et al., 2001), is why hot electrons are seen in only parts of the boundary layer (while hot ions are seen throughout the interval), and why so rarely overall.

3. Statistical Characterization of Ion and Electron Populations

To obtain a global picture of typical ion and electron spectra in the LLBL with respect to location along the magnetopause, we performed a large-scale statistical analysis of the omnidirectional ion and electron fluxes measured by the ESA instruments on board the five THEMIS spacecraft. This will allow us in the next subsections to determine the relevant criteria for identifying the DPBL with the help of automated data mining.

For the statistical analyses in this section we used all available THEMIS data in both the *REDUCED* (3-s time resolution) and *FULL* (96 s) modes, as explained in relevant sections. The periods covered are as follows:

- 1 April 2007 to 24 July 2014 for THEMIS A, D, and E.
- 1 April 2007 to 30 December 2009 for THEMIS B and C; that is, until they became the "Acceleration, Reconnection, Turbulence and Electrodynamics of the Moon's Interaction with the Sun" satellite mission in early 2010 and were sent into orbit around the moon.

3.1. Automated Magnetopause Detection

Performing a statistical study of the LLBL first requires the identification of the magnetopause. For that purpose, we first processed an automated detection algorithm of magnetopause crossings using the online Automated Multi-Dataset Analysis (AMDA) data mining software (http://amda.irap.omp.eu/). Then, we represented the ion and electron spectra with respect to a transition parameter, that is, the ratio n/T where n is the ion density and T the ion temperature, which is often used as a proxy for the spacecraft location relative to the magnetopause (Lockwood & Hapgood, 1997).

The first step for magnetopause crossing automated detection was performed through the analysis of changes in the transition parameter. A candidate was identified and recorded when absolute values of the transition parameter's change on a time scale of 5 min exceeded some set threshold. Five minutes was found to be a good compromise, based on visual inspection of the detection scheme, between magnetopause oscillations (we want to look at effective, large-scale magnetopause crossings and not all the quick and often multiple crossings when the magnetopause oscillates past the spacecraft) and the data resolution of 3 s or 96 s.
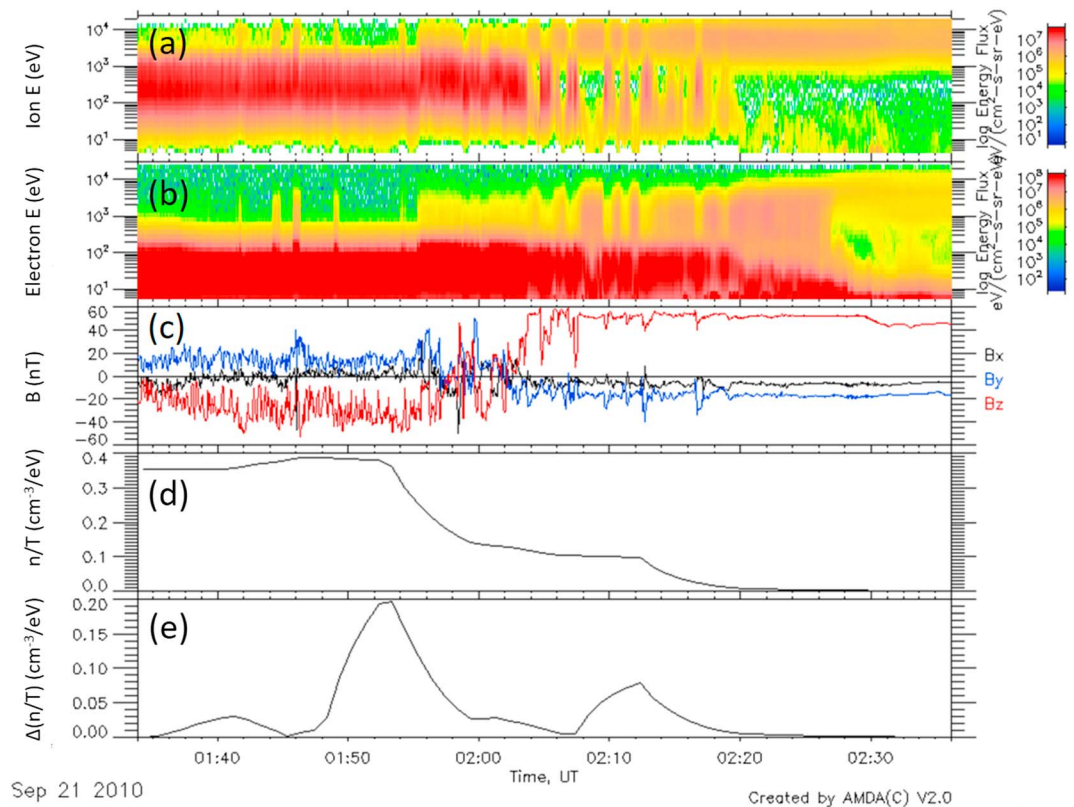
Figure 2. Example of a magnetopause crossing on 21 September 2010, obtained from the AMDA tool (http://amda.irap. omp.eu/). (a) Ion spectrogram. (b) Electron spectrogram. (c) Magnetic field in GSE coordinates. (d) n/T (in cm^{-3}/eV). (e) Δ (n/T; in cm^{-3}/eV).

The threshold used for changes in n/T has been fixed after looking at a large number of magnetopause crossings and chosen high enough so that only unambiguous magnetopause crossings are retained. For our purpose, losing some events (by choosing a conservatively high threshold) is not detrimental as long as the statistics remains sufficient and representative.

The criteria we used for magnetopause crossing event identification are the following:

- $\Delta (n/T)_{5min} = |n/T (t) - n/T (t - 5 \min)| > 0.08$ cm^{-3}/eV
- $7\ R_E < R < 15\ R_E$ (where R is the geocentric distance of the satellite)
- $X_{GSE} > -2\ R_E$

The search provided a catalogue of 4,490 magnetopause crossings. An example crossing (21 September 2010) is illustrated in Figure 2. The figure was made with the AMDA tool, which was used for the automated analysis (http://amda.irap.omp.eu/). It shows the ion and electron spectrogram (panels [a] and [b]), the magnetic field in GSE coordinates (panel [c]) and the transition parameter n/T (in cm^{-3}/eV [panel d]). The variation in transition parameter, which is used for the automated magnetopause detection, is shown Δ (n/T; in cm^{-3}/ eV). Within the 5-min resolution, the magnetopause is correctly identified using this scheme.

Visual examination of some cases and their spatial distribution, however, revealed that the collection of events obtained included some bow shock crossings. A second step was devised with the inclusion of an additional criterion to eliminate bow shock crossings. After having compared the variations of various parameters, the ion temperature was chosen as the additional parameter in our algorithm to get rid of bow shocks. Indeed, temperature changes are systematically and significantly larger across the magnetopause than across the bow shock. After having examined a large number of bow shock and magnetopause crossings, we chose the following threshold (Figure 7) for a magnetopause to be part of our list:

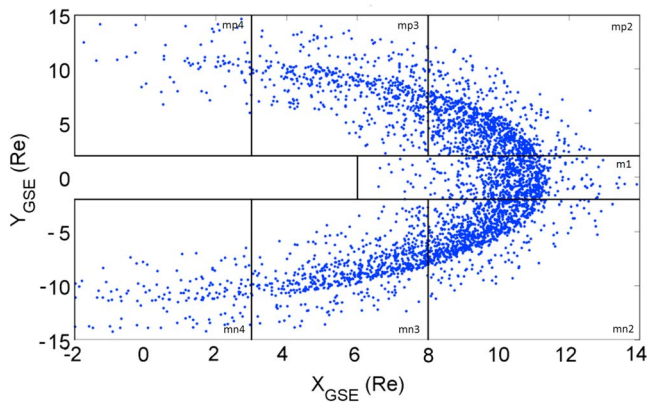- $\Delta (T)5 \min = |T (t) - T (t - 5 \min)| > 500$ eV

Figure 3. Plot of all magnetopause crossings obtained from our automated detection scheme. The seven rectangles show our splitting of the magnetosphere in seven regions that include all the magnetopause crossings (see text for details). The regions are labeled m1 at the nose and then mp2 to mp4 at dusk and mn2 to mn4 at dawn (the *p* and *n* merely refer to positive and negative Y_{GSE}).

This data mining allowed us to obtain a catalogue of 4,490 magnetopause crossings, of which we plotted the locations in Figure 3. One should note that there is an orbital bias favoring crossings at a radius of ~11 R_E because most of the data come from THEMIS A, D, and E, which have an apogee of around 12 R_E.

3.2. Average Characteristics of Ion and Electron Populations

In order to study the characteristics of particle populations as a function of location along the magnetopause, we divided the data set into seven regional areas, going from the nose of the magnetosphere to its flanks (cf. rectangles in Figure 3). Each region has a large number of samples, thereby permitting a statistical study. For this part of the study, we have used omnidirectional energy flux data at high time resolution (3 s) from the *reduced* mode of the ESA instrument.

All magnetopause crossings from our catalogue have been expanded as intervals of 1 hr in duration (30 min before the magnetopause crossing and 30 min after), and all particle spectra were averaged with 1-min time resolution relative to the magnetopause crossing in a superposed epoch analysis. The superposed epoch analysis was made with respect to the transition parameter, and separately for each of the seven sectors, as identified in Figure 3.

The transition parameter was chosen for these representations because it is a good way of ordering magnetopause data to resolve ambiguities otherwise present in the temporal sequence of satellite observations, as often caused by boundary motions (Lockwood & Hapgood, 1997). The data are displayed as energy spectrograms for each figure, where we plot the mean energy fluxes in color as a function of the transition parameter and the particle energy.

As can be seen in Figures 4 and 5, the transition parameter organizes very well the mean spectra in the different regions along the magnetopause. We clearly see the magnetosheath population for high *n/T* and the magnetosphere for low *n/T*. For ions, in Figure 4, we notice the presence of a double population on the dusk flank of the magnetosphere and near the nose for *n/T* values ranging from 10^{-2} to 10^{-3} cm^{-3}/eV. This mixing does not exist on the dawn flank, which supports the hypothesis that these hot ions originate from the tail and have gradient and curvature drifted toward the duskside. By contrast, in Figure 5, the average spectrograms suggest that double peaks are observed less frequently and are not as distinguishable for electrons. Such double peaks are faint but observable near the nose sector (m1; cf. figure captions for labeling explanations) for a small range of *n/T* around 10^{-3} cm^{-3}/eV, and arguably also on the two adjacent dayside sectors (mp2 and mn2). However, they are absent in other areas.

We note that such statistical displays naturally create a smooth transition in the spectra which is not representative of any given magnetopause crossing—individual transitions are typically abrupt. Statistical displays may also spuriously create double populations (separated in energy) if, for example, low-density cold populations are averaged with high-density hot populations in the same *n/T* bin. Nevertheless, on average the presence of double peaks in either ions or electrons should be related to a higher likelihood of observing such double populations in the associated region. In any case, this ambiguity does not affect the analysis performed in the next sections.

We also made a sectorial superposed epoch analysis after separating data according to four IMF orientations in the Y-Z_{GSM} plane (±45° around the north, south, dawn, and dusk directions), using OMNI data. The resulting sets of ion and electron spectrograms as a function of the transition parameter are provided as eight figures in the supporting information.

We do not focus on all the details of Figures S1 to S8, but note two main characteristics of interest for our purpose. First, from the average ion spectra, we see that when the IMF is directed northward (Figure S1 mp4), the double population in the duskside is much more visible than when the IMF is southward (Figure S2 mp4). These are also observed for large IMF B_Y (Figures S3 and S4). Second, for electrons, we again notice that despite the signature being fainter than for ions, double populations are most visible for northward and
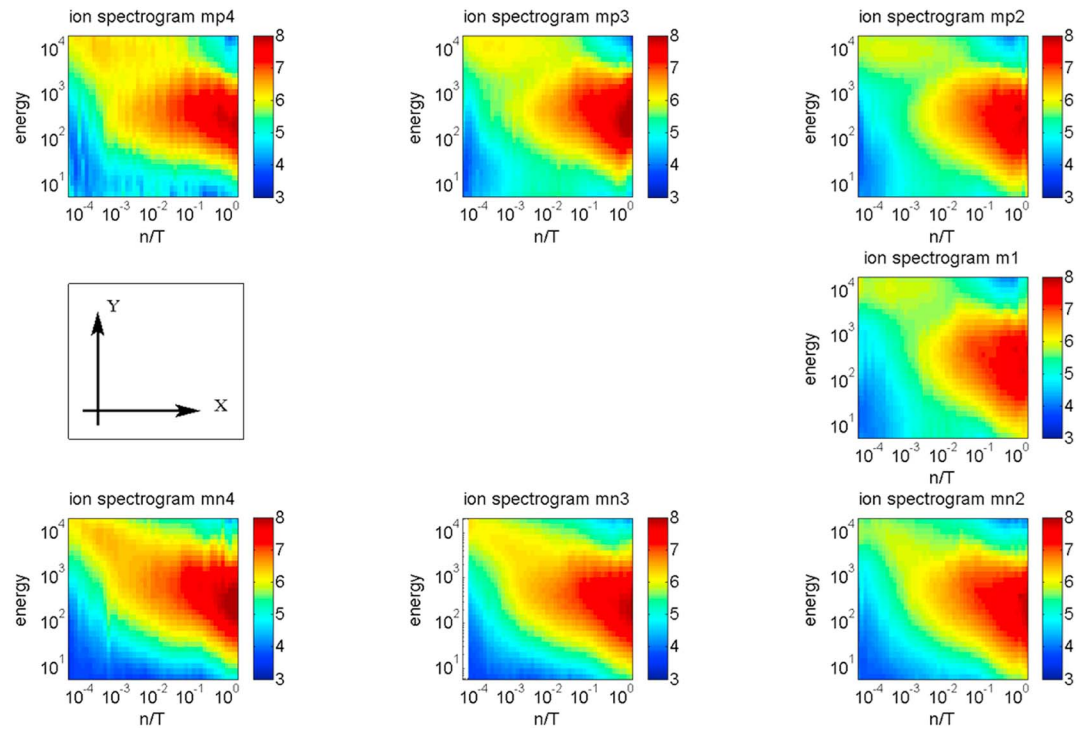
Figure 4. Ion energy spectrograms from a superposed epoch analysis based on the transition parameter (*n/T*), for each of the seven areas defined in Figure 3. On the right-hand side is the spectrogram for the nose of the magnetosphere (m1), the duskside and dawnside magnetopause regions are termed mp2 to mp4 and mn2 to mn4, as already introduced for Figure 3. The color bar indicates the energy flux in log scale, and they are the same for all plots.
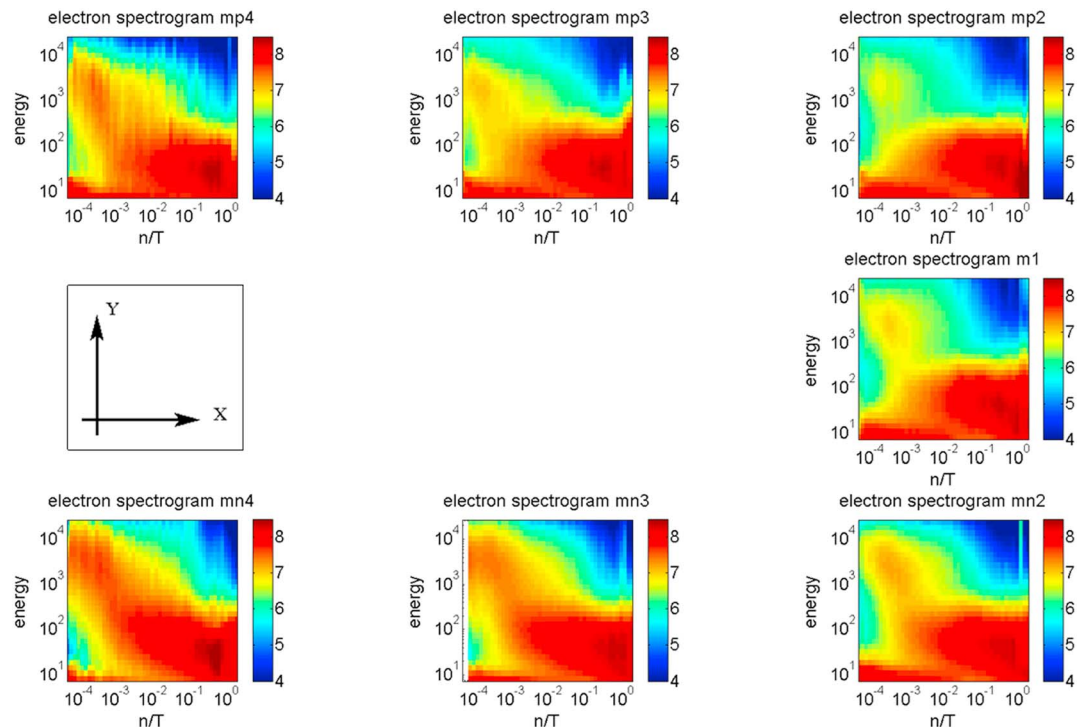

Figure 5. Electron energy spectrograms from a superposed epoch analysis based on the transition parameter (*n/T*), for each of the seven regions (cf. Figure 4 captions for other details).

Table 1
Energy Channels (in eV) Chosen for the Double Population Boundary Layer Search

Ions			Electrons			
M-sphere energy bins	Hole energy bins	M-sheath energy bins	M-sphere energy bins	Hole 1 energy bins	Hole 2 energy bins	M-sheath energy bins
I1	I2	I3	E1	E2	E3	E4
21296.3	7092	1035.4	6788.9	1717.5	28.1	110.5
16178.4	5388	787.2	5157.3	1304.5	20.8	83.9
12290.5	4093	597.5	3917.7	991.8	16.0	63.5
9336.7		453.6	2976.8	752.8		48.5

Note. We call I1 to I3 and E1 to E4 the ensemble of the energy bands used for identifying the populations.

strong IMF B_Y and on the dayside while not on the flanks (regions m1 and mp2 in Figures S5, S7, and S8). In particular, there is no obvious double population at dawn that would constitute the counterpart of the observed double ion populations at dusk (regions mp4 in Figures S5, S7, and S8), given the opposite gradient and curvature drift from the tail for electrons. These trends will be examined in further detail in the discussion section.

4. Statistics of Multiple Ion and Electron Populations

4.1. Selection Criteria

The most commonly observed LLBL include three populations: cold ions and electrons coming from the magnetosheath, and hot ions of magnetospheric origin. More rarely, an additional population of hot electrons can be observed (cf. previous sections). The aim of the present section is to report on the statistical analysis of individual energy spectra in a large-scale fashion, to determine their spatial distribution, occurrence, and how they are ordered by interplanetary conditions (IMF). It should be noted that the magnetosphere also contains even colder ions of ionospheric origin (André & Cully, 2012; Chappell et al., 1987; Sauvaud et al., 2001), but once inside the LLBL they are heated and mostly indistinguishable from ions of magnetosheath origin (Dargent et al., 2017; Toledo-Redondo et al., 2016, 2017). They are thus not addressed in the present study.

The analysis in section 3 allowed us to determine characteristic ion and electron energies for use in an automated search of the DPBL. This search for double peaks in ion and electron populations was then performed directly on energy spectra using 1-min time-averaged THEMIS data (originally with a 3-s time resolution), with the same spacecraft and over the same periods as in section 3. Also using results from section 3, search criteria were built for ions and electrons such that given energy flux thresholds are required in specific energy ranges. The energy ranges chosen to best identify each type of population are given in Table 1. These energy ranges (three for ions—I1 to I3—and four for electrons—E1 to E4) are also displayed as black rectangles in Figure 6, which shows all energy spectra with double peaks superposed on the same plots for (a) ions and (b) electrons. As can be already understood, the idea of our data mining simply relies on the use of energy flux thresholds in (and ratios between) different energy ranges to ensure the presence or absence of a given peak in the spectra. It should be noted that a second *hole* energy band is used for electrons at low energies (hole 2 or E2). This criterion was added in order to distinguish true magnetosheath electrons (with low flux at very low energies) from ionospheric electrons (which can sometimes have significant fluxes at magnetosheath energies but also have large fluxes at very low energies owing to a temperature lower than magnetosheath-like electrons).

The automated search for concomitant double populations (two peaks) in both ions and electrons was then performed with the following criteria (where J_E is the average energy flux in given energy bands):

- Ion double population:
  - J_E (I1 & I3) $> 10^5$ eV/(cm^2.s.sr. eV)
  - J_E (I2)/J_E (I1) and J_E (I2)/J_E (I3) $< 90\%$
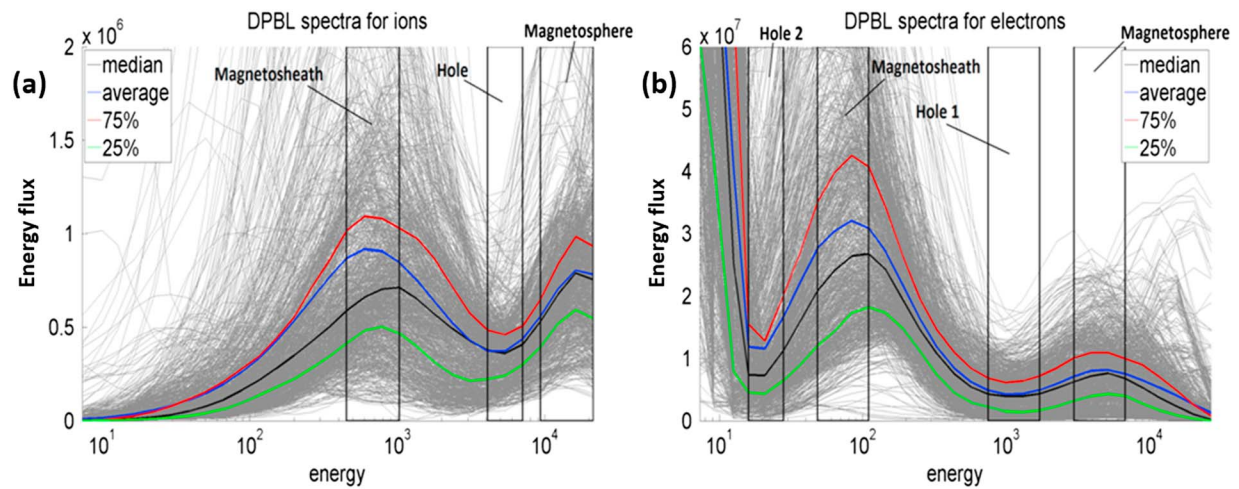- Electron double population:

Figure 6. (a) Ion and (b) electron spectra of all the double population boundary layer (DPBL) events (every gray line is a spectrum from 1-min-averaged Time History of Events and Macroscale Interactions during Substorms data). The boxes are the energy ranges used to characterize each population (magnetosphere and magnetosheath) and *holes* that we have chosen (including the low energy *hole 2* used for electrons just above the photoelectrons) for the data mining. Medians, averages, and percentile curves are also given in various colors, as labeled.

— J_E (E1) $> 10^5$ eV/(cm^2.s.sr. eV) and J_E (E4) $> 10^6$ eV/(cm^2.s.sr. eV)
— J_E (E2)/J_E (E1) & J_E (E2)/J_E (E4) and J_E (E3)/J_E (E4) $< 90\%$

This data mining finds many double peaks in isolated 1-min samples (the data sampling resolution). Since the original time resolution is 3 s, most cases may result from time aliasing in the averaging process; that is, a double peak profile may come from the averaging of magnetosheath and magnetosphere energy fluxes which may otherwise not be mixed if looking at higher time resolutions (below the 1-min averaging). For this reason, we removed all 1-min intervals from our analysis (even if we do not free ourselves from the same problem if the magnetopause is oscillating during more than 1 min, but this is in any case much rarer).
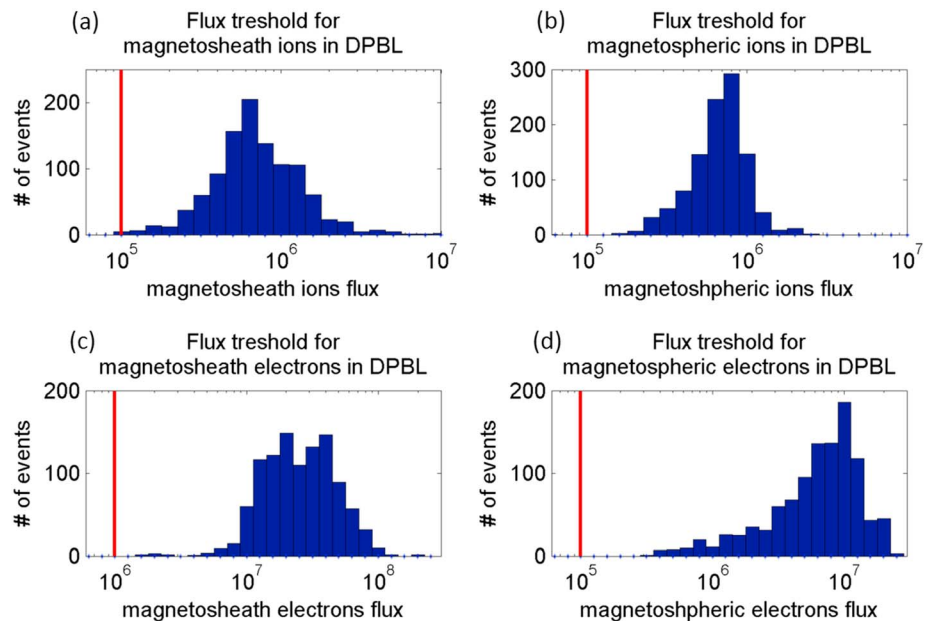
Figure 7. Distributions of the energy flux thresholds (eV/(cm^2.s.sr. eV)) used in the data mining analysis for each ion (a,b) and electron (c,d) population (magnetosheath and magnetosphere). The threshold used for searching DPBL events is given in each case with a vertical red line. DPBL = double population boundary layer.
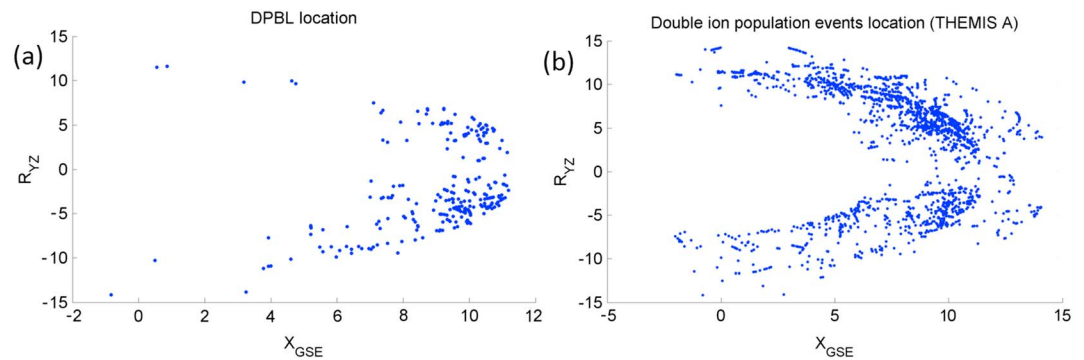
Figure 8. X-Y_{GSE} plane spatial distribution of (a) double population boundary layer (DPBL) and (b) double ion population events. THEMIS A = Time History of Events and Macroscale Interactions during Substorms A.

Figure 6 confirms that the energy channels we chose fit well the typical double peaks and holes in energy flux measured during DPBL observations. Figure 7 shows the distribution of particle energy fluxes in the energy ranges relevant to the two main populations (magnetosphere and magnetosheath) for the data set that has two peaks in both ions and electrons. The threshold used (as presented above) is shown with a red vertical line in each panel. The fact that the threshold is well below the core of the energy flux distribution confirms that these thresholds are appropriate for our purpose, that is, so that we should detect most of the DPBL events.

4.2. Spatial Distribution of DPBL Events

Now we first visualize the X-Y_{GSE} plane spatial distribution of the DPBL events in Figure 8a and then analyze the difference between the occurrence distribution of DPBL events along the x axis with that of all magnetopause crossings from our data set in Figure 9a. We first notice in Figure 8a a slight dawn-dusk asymmetry in the DPBL observations, with more events at dawn (997) than at dusk (466). We believe that this trend may be a result of the need for a well-defined high-energy electron population in our selection criteria, while it is known that high-energy electrons drift around the dawnside of the magnetosphere to access the dayside regions. It should also be noted that there may be more than one DPBL event per magnetopause crossing (from the automatic detection scheme).

Figure 9a shows, on the other hand, that the likelihood of observation of the DPBL is significantly higher at the subsolar magnetopause than further down the flanks, when compared to all magnetopause crossings. The red histogram (DPBL events) does not follow the same trend as the blue histogram (all magnetopause). It is significantly more peaked on the dayside. This result is consistent with the large-scale superposed epoch analysis of electron spectra in section 3, which also showed that double electron populations are mostly recorded in the dayside area.
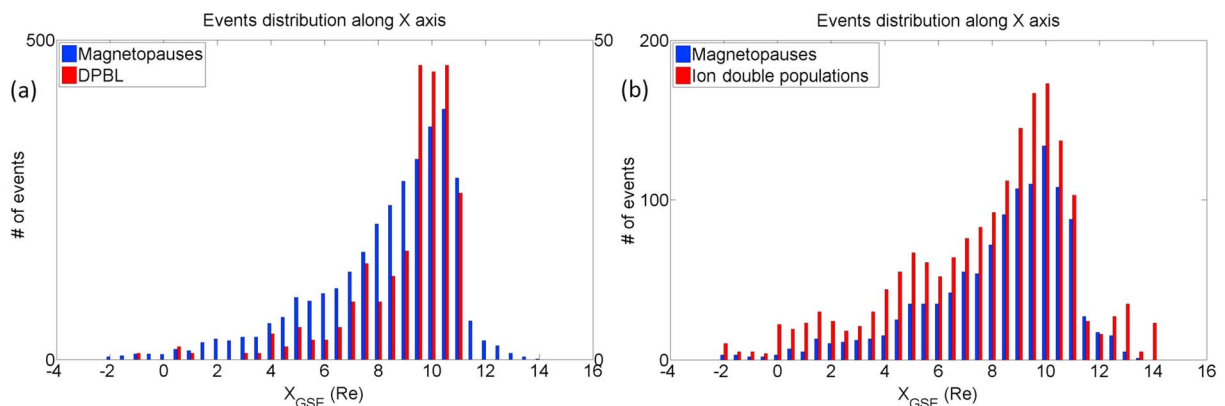

Figure 9. X_{GSE} spatial distribution of (a) double population boundary layer (DPBL) and (b) double ion population events, both as red histograms in panels (a) and (b), while the distribution of all magnetopause crossings is given in each as a blue histogram.
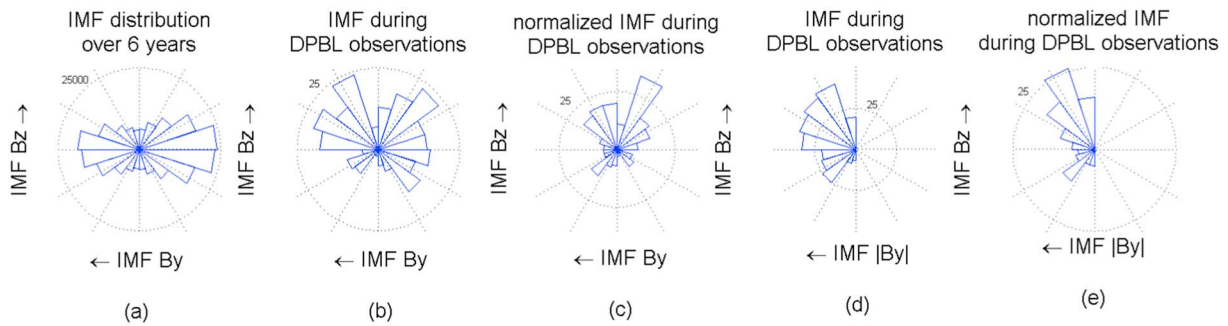
Figure 10. Interplanetary magnetic field (IMF) clock angle angular distributions for (a) all 6 years of observations, (b) during double population boundary layer (DPBL) events, and (c) the normalized distribution for DPBL events (i.e., [b] normalized to [a]). Panels (d) and (e) display the same distributions as (b) and (c) but only for the norm of the IMF B_Y. Scales are given in each angular distribution with a number next to a circle of given radius.

To further demonstrate the significance of these DPBL spatial distributions, we performed in parallel a smaller survey using only THEMIS A data (surveyed over the same 7 years) to search for double ion populations alone, that is, with no concomitant double peaks in electron spectra (this subset retains significant statistics, yet its survey was easier to perform). The results of this smaller survey are given in Figures 8b and 9b, in the same format as Figures 8a and 9a. From these distributions we observe that unlike the DPBL, observations of double ion populations alone have no dependence on the location along the x axis, in the sense that they follow the same trend as the distribution of all magnetopause crossings. These findings are further discussed in section 5.

Finally, it should be noted that we found 1,880 double ion population events and 111 DPBL during this smaller survey on 7 years of THEMIS A alone. Average durations of the double ion populations are 4:50 min, while DPBL events average duration is 3:28 min. Double ion population observations are thus generally longer and more common. DPBL observations represent only 6% of all double ion populations in this smaller survey.

4.3. DPBL Occurrence Distribution as a Function of IMF Orientation

As alluded previously, the IMF orientation is suspected to be a key parameter for the DPBL formation process, especially with respect to the high-latitude reconnection model.

As we are interested in the IMF conditions prevailing during the formation of the DPBL, we used IMF measurements from the OMNI data set (https://omniweb.gsfc.nasa.gov/) averaged over the DPBL time intervals extended by 5 min preceding each event (the overall results do not change if using other sensible averaging intervals). Figure 10 shows the distribution of IMF conditions in several formats. It shows the IMF clock angle distributions for (a) all 6 years of observations, (b) during DPBL events, and (c) the normalized distribution for DPBL events (i.e., [b] normalized to the IMF distribution in panel [a]). Figures 10d and 10e display the same distributions as (b) and (c) but only for the norm of the IMF B_Y. All these distributions consistently show that DPBL events are typically observed when the IMF is northward but with a significant B_Y component.

5. Discussion

Several processes may be considered to explain the presence of hot magnetospheric electrons in the dayside boundary layers and the formation of such DPBL, as follows.

1. Local diffusion (wave-particle interactions): a purely diffusive process is unlikely as discussed later.
2. Local entry through the KH instability (Hasegawa et al., 2004; Miura, 1994). This process cannot explain DPBL observations because no large velocity shear is typically observed nor expected at such dayside locations.
3. Diffusive entry or KH further downtail, followed by sunward convection along the magnetopause. This process is also deemed unlikely because this would not result in a thin boundary layer attached to the magnetopause on the dayside, and furthermore, sunward flows are rarely observed in the flank LLBL and DPBL.
4. Capture of magnetosheath plasma by double high-latitude reconnection (Lavraud et al., 2006; Song & Russell, 1992). This process can explain the presence of counterstreaming and heated magnetosheath
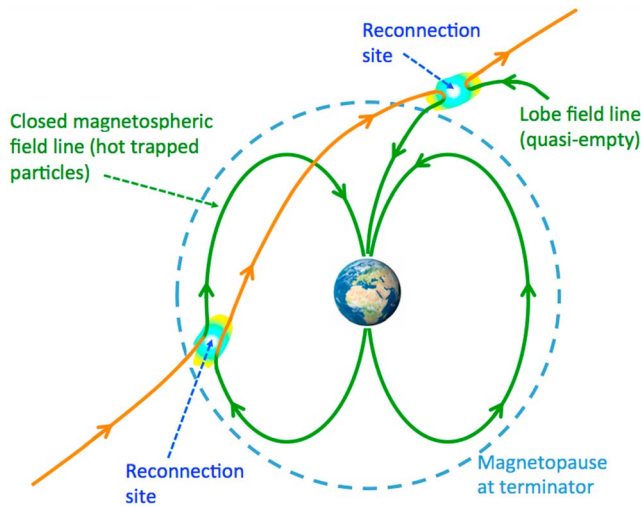
Figure 11. Sketch representing double reconnection of a magnetosheath field line with empty lobe field line at one end and a closed magnetospheric field line at the other end. The latter contains hot electrons which can then populate the newly closed field line on the dayside (unlike the case of double high-latitude reconnection with only lobe field lines at both ends, with are devoid of such hot electrons).

electrons in the LLBL (cf. introduction), but it does not explain the presence of hot ions and electrons. The presence of hot ions has often been related to gradient and curvature drift, from the tail toward the dusk LLBL where double ion populations are often observed (e.g., Hasegawa et al., 2003), as also exemplified in Figure 8b. This process should allow a similar mixing for electrons, but on the dawnside (owing to oppositely directed gradient and curvature drifts for electrons). However, our analysis has demonstrated that double electron populations are rarely observed, even on the dawnside.

5. Another possibility is the capture of magnetosheath plasma onto closed field lines by reconnection tailward of the cusp in one hemisphere and equatorward of the cusp in the other hemispheres with previously closed field lines (which already contain hot electrons; Øieroset et al., 2008). This process is the most likely, as argued below.

Based on our statistical surveys, we showed that DPBL observations are roughly 17 times less frequent than boundary layers with mixed ions but no mixed electrons (equivalently they represent only 6%). The occurrence of mixed ion populations is very high on the dusk flank (Hasegawa et al., 2003) and its relative occurrence when normalized to all magnetopause crossings in our statistical study does not show a dependence on distance downtail. By contrast, if we take a look at the location of our DPBL events, we notice that the likelihood of observations is clearly higher at the subsolar magnetopause than further down the flanks. The process leading to its formation is thus unlikely related to processes occurring preferentially downtail, such as the KH instability.

The key process may thus be magnetic reconnection. For purely northward IMF and reconnection in the lobes tailward of both cusps, the resulting newly closed field lines are only expected to contain ions and electrons of magnetosheath energies (though slightly heated). This is because lobe field lines are mostly empty of plasma. An efficient way of mixing plasma of solar origin with both hot ions and electrons of magnetospheric origin would, however, be to reconnect at least one end of the IMF field line with a field line that was previously closed and filled with hotter magnetospheric plasma. This may be done if there is a sufficient Y component in the IMF orientation so that an IMF field line may reconnect in the lobe in one hemisphere but more on the side of the magnetosphere and at lower latitude in the other hemisphere with a previously closed field line (already containing a source of hot magnetospheric ions and electrons). Note that this scenario was previously suggested to explain double ion populations at low altitudes in the cusp region (e.g., Chandler et al., 2008). This double reconnection process is sketched in Figure 11. Such characteristics are consistent with our statistical results, which found an increased DPBL occurrence at the dayside magnetopause and for dominant IMF B_Y. The case study shown in Figure 1 is also consistent with this hypothesis since the IMF B_Y is around 4 nT with a clock angle varying between 30° and 70°.

An open issue remains the systematic presence of hot ions but the rare presence of hot electrons in dayside boundary layers. This is true in particular on the dayside where the gradient and curvature drift explanation discussed before cannot hold; there is no reason for hot electrons not to (curvature and gradient) drift into subsolar boundary layers like ions appear to do very frequently, albeit through the dawn instead of the duskside. These facts suggest that a diffusive process must also be active and that it is much more efficient for ions (which have a larger gyroradius), while electrons require a double reconnection process as explained above to populate the boundary layers.

Another hypothetic scenario that must be mentioned is as follows. Assume reconnection in one hemisphere occurs with a dayside closed field line and the other end reconnects with an empty lobe field line. Then, if reconnection occurs first with the lobe field lines, when reconnection occurs in the other hemisphere with the closed field line all the hot magnetospheric plasma will remain trapped on the newly closed field line (providing the explanation for DPBL observations). However, if the temporal sequence is opposite, so that

the dayside closed field line reconnects with a solar wind field line first, then hot electrons are so fast that they may escape into the solar wind in a matter of seconds to minutes before the other end of the field line reconnects with the empty lobe field line in the other hemisphere. In such a case, a boundary layer with hot ions but no hot electrons would be formed, since hot ions are much slower than hot electrons. This scenario should further contribute to the observed low occurrence rate of DPBL events.

Another result that strengthens this double reconnection model is the energy flux distribution of the hot magnetospheric electron population in our DPBL (Figure 7d). The fact that there are no DPBL observations in the flux range 10^5–10^6 is consistent with the idea of double reconnection with a closed magnetospheric field line in the sense that hot electrons suddenly find themselves on a new, closed field line, but without any significant change in fluxes. This contrasts with what would be expected from a more diffusive process.

6. Conclusions

We performed several types of large-scale statistical analyses with the purpose of finding the origin of the rare observation of concomitant double ion and electron populations in the dayside magnetopause boundary layers (termed DPBL for Double Population Boundary Layers).

Our findings reveal that the DPBL are encountered predominantly near the nose of the magnetosphere. This differentiate them from the double ion population boundary layers, which are located equally on the nose of the magnetosphere and on its dusk flanks. DPBL is also much less frequent than double ion populations (6%). A statistical study of the IMF orientation has revealed that DPBL events form preferentially under northward IMF but with a significant B_Y component. This is interpreted as a result of reconnection of the same magnetosheath field line in both hemispheres, but with at least one end reconnecting in its hemisphere at lower latitude with a closed magnetospheric field line that already contains a hot electron source.

References

André, M., & Cully, C. M. (2012). Low-energy ions: A previously hidden solar system particle population. *Geophysical Research Letters*, *39*, L03101. https://doi.org/10.1029/2011GL050242

Auster, H.-U., Glassmeier, K. H., Magnes, W., Aydogar, O., Baumjohann, W., Constantinescu, D., et al. (2008). The THEMIS fluxgate magnetometer. *Space Science Reviews*, *141*(1-4), 235–264. https://doi.org/10.1007/s11214-008-9365-9

Badman, S. V., Masters, A., Hasegawa, H., Fujimoto, M., Radioti, A., Grodent, D., et al. (2013). Bursty magnetic reconnection at Saturn's magnetopause. *Geophysical Research Letters*, *40*, 1027–1031. https://doi.org/10.1002/grl.50199

Chandler, M. O., Avanov, L. A., Craven, P. D., Mozer, F. S., & Moore, T. E. (2008). Observations of the ion signatures of double merging and the formation of newly closed field lines. *Geophysical Research Letters*, *35*, L10107. https://doi.org/10.1029/2008GL033910

Chappell, C. R., Moore, T. E., & Waite, J. H. (1987). The ionosphere as a fully adequate source of plasma for the Earth's magnetosphere. *Journal of Geophysical Research*, *92*(A6), 5896–5910. https://doi.org/10.1029/JA092iA06p05896

Cowley, S. W. H. (1981). In B. Hultqvist & T. Hagfors (Eds.), *Interpretation of observed relations between solar wind characteristics and effects at ionospheric altitudes, High-latitude space plasma physics* (pp. 225–249). Plenum Press.

Dargent, J., Aunai, N., Lavraud, B., Toledo-Redondo, S., Shay, M. A., Cassak, P. A., & Malakit, K. (2017). Kinetic simulation of asymmetric magnetic reconnection with cold ions. *Journal of Geophysical Research: Space Physics*, *122*, 5290–5306. https://doi.org/10.1002/2016JA023831

Dungey, J. W. (1961). Interplanetary magnetic field and the auroral zones. *Physical Review Letters*, *6*(2), 47–48. https://doi.org/10.1103/PhysRevLett.6.47

Fairfield, D. H., Otto, A., Mukai, T., Kokubun, S., Lepping, R. P., Steinberg, J. T., et al. (2000). Geotail observations of the Kelvin-Helmholtz instability at the equatorial magnetotail boundary for parallel northward fields. *Journal of Geophysical Research*, *105*(A9), 21,159–21,173. https://doi.org/10.1029/1999JA000316

Foullon, C., Farrugia, C. J., Fazakerley, A. N., Owen, C. J., Gratton, F. T., & Torbert, R. B. (2008). Evolution of Kelvin-Helmholtz activity on the dusk flank magnetopause. *Journal of Geophysical Research*, *113*, A11203. https://doi.org/10.1029/2008JA013175

Fuselier, S. A., Anderson, B. J., & Onsager, T. G. (1995). Particle signatures of magnetic topology at the magnetopause: AMPTE/CCE observations. *Journal of Geophysical Research*, *100*(A7), 11,805–11,822. https://doi.org/10.1029/94JA02811

Fuselier, S. A., Anderson, B. J., & Onsager, T. G. (1997). Electron and ion signatures of field line topology at the low shear magnetopause. *Journal of Geophysical Research*, *102*(A3), 4847–4863. https://doi.org/10.1029/96JA03635

Fuselier, S. A., Frahm, R., Lewis, W. S., Masters, A., Mukherjee, J., Petrinec, S. M., & Sillanpaa, I. J. (2014). The location of magnetic reconnection at Saturn's magnetopause—A comparison with Earth. *Journal of Geophysical Research: Space Physics*, *119*, 2563–2578. https://doi.org/10.1002/2013JA019684

Fuselier, S. A., Petrinec, S. M., Trattner, K. J., & Lavraud, B. (2014). Magnetic field topology for northward IMF reconnection: Ion observations. *Journal of Geophysical Research: Space Physics*, *119*, 9051–9071. https://doi.org/10.1002/2014JA020351

Fuselier, S. A., Trattner, K. J., Petrinec, S. M., & Lavraud, B. (2012). Dayside magnetic topology at the Earth's magnetopause for northward IMF. *Journal of Geophysical Research*, *117*, A08235. https://doi.org/10.1029/2012JA017852

Gosling, J. T., Thomsen, M. F., Bame, S. J., Elphic, R. C., & Russell, C. T. (1991). Observations of reconnection of interplanetary and lobe magnetic field lines at the high-latitude magnetopause. *Journal of Geophysical Research*, *96*(A8), 14,097–14,106. https://doi.org/10.1029/91JA01139

Hasegawa, H., Fujimoto, H., Maezawa, K., Saito, Y., & Mukai, T. (2003). Geotail observation of the dayside outer boundary region: Interplanetary magnetic field control and dawn-dusk asymmetry. *Journal of Geophysical Research*, *108*(A4), 1163. https://doi.org/10.1029/2002JA009667

Hasegawa, H., Fujimoto, M., Phan, T.-D., Rème, H., Balogh, A., Dunlop, M. W., et al. (2004). Transport of solar wind into Earth's magnetosphere through rolled-up Kelvin-Helmholtz vortices. *Nature*, *430*(7001), 755–758. https://doi.org/10.1038/nature02799

Kessel, R. L., Chen, S.-H., Green, J. L., Fung, S. F., Boardsen, S. A., Tan, L. C., et al. (1996). Evidence of high-latitude reconnection during northward IMF: Hawkeye observations. *Geophysical Research Letters*, *23*, 586.

Lavraud, B., Dunlop M. W., Phan T. D., Rème H., Bosqued J. M., Dandouras I., et al. (2002). Cluster observations of the exterior cusp and its surrounding boundaries under northward IMF. *Geophysical Research Letters*, *29*(20), 1995. https://doi.org/10.1029/2002GL015464

Lavraud, B., Fedorov, A., Budnik, E., Thomsen, M. F., Grigoriev, A., Cargill, P. J., et al. (2005). High-altitude cusp flows dependence on IMF orientation: A three-year Cluster statistical study. *Journal of Geophysical Research*, *110*, A02209. https://doi.org/10.1029/2004JA010804

Lavraud, B., Thomsen, M. F., Lefebvre, B., Schwartz, S. J., Seki, K., Phan, T. D., et al. (2006). Evidence for newly closed magnetosheath field lines at the dayside magnetopause under northward IMF. *Journal of Geophysical Research*, *111*, A05211. https://doi.org/10.1029/2005JA011266

Lavraud, B., Thomsen, M. F., Taylor, M. G. G. T., Wang, Y. L., Phan, T. D., Schwartz, S. J., et al. (2005). Characteristics of the magnetosheath electron boundary layer under northward interplanetary magnetic field: Implications for high-latitude reconnection. *Journal of Geophysical Research*, *110*, A06209. https://doi.org/10.1029/2004JA010808

Li, W., Raeder, J., Thomsen, M. F., & Lavraud, B. (2008). Solar wind plasma entry into the magnetosphere under northward IMF conditions. *Journal of Geophysical Research*, *113*, A04204. https://doi.org/10.1029/2007JA012604

Lockwood, M., & Hapgood, M. A. (1997). How the magnetopause transition parameter works. *Geophysical Research Letters*, *24*(4), 373–376. https://doi.org/10.1029/97GL00120

McAndrews, H. J., Owen, C. J., Thomsen, M. F., Lavraud, B., Coates, A. J., Dougherty, M. K., & Young, D. T. (2008). Evidence for reconnection at Saturn's magnetopause. *Journal of Geophysical Research*, *113*, A04210. https://doi.org/10.1029/2007JA012581

McFadden, J. P., Carlson, C. W., Larson, D., Ludlam, M., Abiad, R., Elliott, B., et al. (2008). The THEMIS ESA plasma instrument and in-flight calibration. *Space Science Reviews*, *141*(1-4), 277–302. https://doi.org/10.1007/s11214-008-9440-2

Nykyri, K., Otto, A., Lavraud, B., Mouikis, C., Kistler, L. M., Balogh, A., & Reme, H. (2006). Cluster observations of reconnection due to the Kelvin-Hemholtz instability at the dawnsdie magnetospheric flank. *Annales de Geophysique*, *24*(10), 2619–2643. https://doi.org/10.5194/angeo-24-2619-2006

Ogino, T., Walker, R. J., & Ashour-Abdalla, M. (1994). A global magnetohydrodynamic simulation of the response of the magnetosphere to a northward turning of the interplanetary magnetic field. *Journal of Geophysical Research*, *99*(A6), 11027. https://doi.org/10.1029/93JA03313

Øieroset, M., Phan, T. D., Angelopoulos, V., Eastwood, J. P., McFadden, J., Larson, D., et al. (2008). THEMIS multi-spacecraft observations of magnetosheath plasma penetration deep into the dayside low-latitude magnetosphere for northward and strong By IMF. *Geophysical Research Letters*, *35*, L17S11. https://doi.org/10.1029/2008GL033661

Onsager, T. G., Scudder, J. D., Lockwood, M., & Russell, C. T. (2001). Reconnection at the high latitude magnetopause during northward interplanetary magnetic field conditions. *Journal of Geophysical Research*, *106*(A11), 25,467–25,488. https://doi.org/10.1029/2000JA000444

Paschmann, G., Sonnerup, B. U. Ö., Papamastorakis, I., Sckopke, N., Haerendel, G., Bame, S. J., et al. (1979). Plasma acceleration at the Earth's magnetopause—Evidence for reconnection. *Nature*, *282*(5736), 243–246. https://doi.org/10.1038/282243a0

Raeder, J., Berchem, J., Ashour-Abdalla, M., Frank, L. A., Paterson, W. R., Ackerson, K. L., et al. (1997). Boundary layer formation in the magnetotail: Geotail observations and comparisons with a global MHD simulation. *Geophysical Research Letters*, *24*(8), 951–954. https://doi.org/10.1029/97GL00218

Sauvaud, J.-A., Lundin, R., Rème, H., McFadden, J. P., Carlson, C., Parks, G. K., et al. (2001). Intermittent thermal plasma acceleration linked to sporadic motions of the magnetopause, first cluster results. *Annales de Geophysique*, *19*(10/12), 1523–1532. https://doi.org/10.5194/angeo-19-1523-2001

Song, P., & Russell, C. T. (1992). Model of the formation of the low-latitude boundary layer for strongly northward interplanetary magnetic field. *Journal of Geophysical Research*, *97*(A2), 1411–1420. https://doi.org/10.1029/91JA02377

Taylor, M. G. G. T., & Lavraud, B. (2008). Observation of three distinct ion populations at the Kelvin-Helmholtz-unstable magnetopause. *Annales de Geophysique*, *26*(6), 1559–1566. https://doi.org/10.5194/angeo-26-1559-2008

Toledo-Redondo, S., Andre, M., Khotyaintsev, Y. V., Lavraud, B., Vaivads, A., Graham, D. B., et al. (2017). Energy budget and mechanisms of cold ion heating in asymmetric magnetic reconnection. *Journal of Geophysical Research*, *122*, 9396–9413. https://doi.org/10.1002/2017JA024553

Toledo-Redondo, S., Andre, M., Vaivads, A., Khotyaintsev, Y. V., Lavraud, B., Graham, D. B., et al. (2016). Cold ion heating at the dayside magnetopause during magnetic reconnection. *Geophysical Research Letters*, *43*, 58–66. https://doi.org/10.1002/2015GL067187

Treumann, R. A., Labelle, J., & Bauer, T. M. (1995). *Diffusion processes: An observational perspective*, Geophysical Monograph Series (Vol. 90, p. 331). Washington DC: American Geophysical Union.

Wing, S., Johnson, J. R., Chaston, C. C., Echim, M., Escoubet, C. P., Lavraud, B., et al. (2014). Review of solar wind entry into and transport within the plasma sheet. *Space Science Reviews*, *184*(1-4), 33–86. https://doi.org/10.1007/s11214-014-0108-9